International Journal of Innovative Computing, Information and Control
Volume **22**, Number **3**, June **2026**

ICIC International ©2026 ISSN 1349-4198
pp. **701–721**

MINIMUM SURFACE FOR TRAPEZOIDAL COMBINED FOOTINGS: THE SOIL CONTACT AREA IS PARTIALLY COMPRESSED

Rosa Margarita Luévanos-Soto[1], Arnulfo Luévanos-Rojas[1,*] and Inocencio Luévanos-Soto[2]

[1]Instituto de Investigaciones Multidisciplinaria
Facultad de Contaduría y Administración
Universidad Autónoma de Coahuila, Unidad Torreón
Blvd. Revolución 151 Ote. CP 27000, Torreón, Coahuila, México
r_luevanos@uadec.edu.mx; *Corresponding author: arnulfoluevanos@uadec.edu.mx

[2]Facultad de Ingeniería, Ciencias y Arquitectura
Universidad Juárez del Estado de Durango, Unidad Gómez Palacio
Av. Universidad S/N, Fracc. Filadelfia, CP 35010, Gómez Palacio, Durango, México
inocencio.luevanos@ujed.mx

Received October 2025; revised February 2026

Abstract. *This article shows a model to determine the minimum contact area with the soil for trapezoidal combined footings considering that the area is partially compressed, i.e., a part of the contact area under the footing with the soil is subject to compression and the other part has zero pressure. Some works present the minimum contact area for trapezoidal combined footings, but the contact area of the footing with the soil is completely compressed. The methodology is developed by integration to determine the equations of the resultant force and the moments on the X and Y axes for the five cases of biaxial bending, and four cases of uniaxial bending (two on the X axis and two on the Y axis). Several studies are developed to determine the minimum contact area with the soil for trapezoidal combined footings subjected to biaxial bending and uniaxial bending in each column. The proposed model shows a significant reduction in the minimum contact area with the soil of up to 65.30% for biaxial bending and up to 48.68% for uniaxial bending compared to other studies. The model can be used as a review to minimize the allowable load capacity of the soil (objective function) and the same constraint functions for biaxial or uniaxial bending.*

Keywords: Minimum contact area, Trapezoidal combined footings, Uniaxial bending, Biaxial bending, Contact area partially compressed

1. **Introduction.** A foundation is the set of structural elements of a structure whose purpose is to transmit its loads or those of elements supported on it to the ground, distributing them in such a way that they do not exceed their allowable pressure.

The three main types of foundations are shallow, deep, and semi-deep, each designed to distribute a structure's load on the ground differently. Shallow foundations are used in shallow soils, deep foundations in soils that require greater stress distribution at greater depths (such as with piles), and semi-deep foundations offer intermediate solutions between the two, depending on the soil characteristics and the load on the structure.

Reinforced concrete foundations can be 1) isolated footings supporting a column with square, rectangular, circular and elliptical shapes; 2) combined footings that support two or more columns with rectangular, trapezoidal, elliptical, T and L shapes; 3) strip footings

DOI: 10.24507/ijicic.22.03.701

that support concrete or masonry walls; 4) rafts or foundation slabs that support an entire building.

The dimensions of a foundation for different shapes have been studied by various researchers to estimate the contact area with the ground: for isolated footings [1-6]; for combined footings [7-16]; for foundation slabs [17]. These articles assume that the contact area with the ground is completely compressed.

Now, the published articles assume the minimum contact area with the ground considering that the area is partially compressed: for isolated footings [18-28]; for combined footings [29-32]; for strip footings [33].

The published articles that are most closely related to the topic of TCFs (trapezoidal combined footings) are as the following. Luévanos-Rojas [9] presented the equations to determine the dimensions of the boundary TCFs located at the boundaries of the terrain, but the area is completely compressed. Pasillas-Orona et al. [15] developed a model to determine the minimum area for TCFs considering that the area is fully compressed.

The advantage of using the contact area with the ground when the footing area is partially compressed is that it generates a smaller volume of soil extraction and therefore reduces the cost.

Thus, there is no paper on the topic with the level of current knowledge on a model to estimate the minimum area for TCFs considering that the area is partially compressed.

This article presents a model to estimate the minimum contact area with the soil for TCFs considering that the area is partially compressed (a part of the contact area under the footing with the soil is under compression and the other part has zero pressure). Some papers show the minimum area for TCFs, but the contact area of the footing with the soil is completely compressed. The equations are developed for the resultant force and the moments on the X and Y axes for the five cases of biaxial bending, and four cases of uniaxial bending (two on the X axis and two on the Y axis). Several studies are developed to find the minimum contact area with the soil for TCFs subjected to biaxial bending and uniaxial bending in each column to observe the results.

The paper is organized as follows. Section 2 presents the formulation of the model to determine the minimum area of a TCF using the current model (fully compressed area) and the new model (partially compressed area). Subsection 2.1 describes the equations for biaxial bending in each column of the five cases. Subsection 2.2 shows the equations for uniaxial bending in each column of the four cases. Subsection 2.3 describes the equations for determining the minimum area. Section 3 shows the numerical studies applied to the two models for a TCF. Section 4 describes the results. Section 5 indicates the conclusions to complete the paper.

2. **Formulation of the Model.** The pressure generated by the soil (biaxial bending equation) at any part of a combined footing is determined as follows:

$$\sigma = \frac{R}{A} + \frac{M_{xT}y}{I_x} + \frac{M_{yT}x}{I_y} \tag{1}$$

where σ is the pressure generated by the soil at any part of the footing used in case I $\left(\text{kN/m}^2\right)$, R is the resultant force (kN), A is the area of the base of the footing in plan $\left(\text{m}^2\right)$, M_{xT} is the resultant moment with respect to the X axis (kN-m), M_{yT} is the resultant moment with respect to the Y axis (kN-m), x and y are the coordinates of the pressure point under study (m), and I_x and I_y are the moments of inertia on the X and Y axes $\left(\text{m}^4\right)$.

Figure 1 presents the overall dimensions for a TCF supporting two columns.

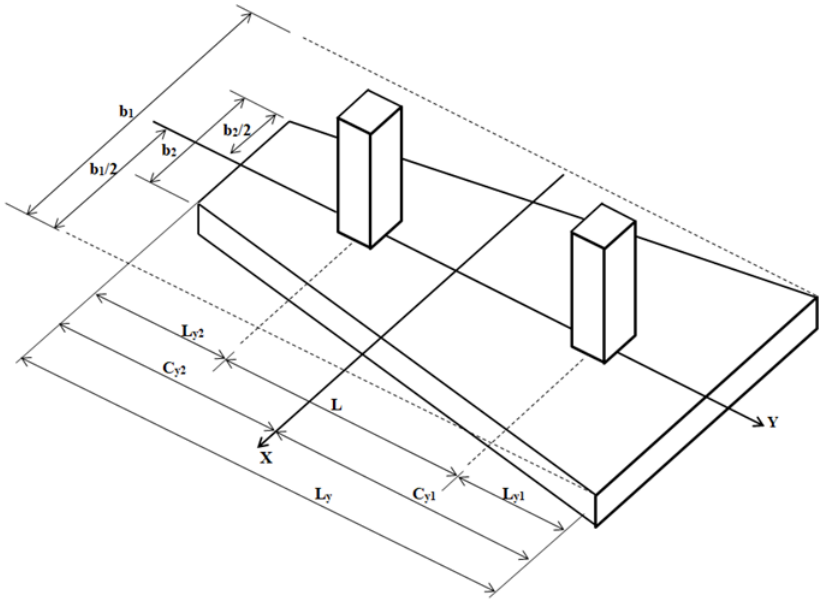

FIGURE 1. Trapezoidal combined footing

The rigid TCF is deformed in planar form, i.e., a linear soil pressure distribution under the footing is considered.

The geometric properties of a trapezoidal footing are

$$A = \frac{L_y(b_1 + b_2)}{2} \tag{2}$$

$$C_{y1} = \frac{L_y(b_1 + 2b_2)}{3(b_1 + b_2)} \tag{3}$$

$$C_{y2} = \frac{L_y(2b_1 + b_2)}{3(b_1 + b_2)} \tag{4}$$

$$I_x = \frac{{L_y}^3\left({b_1}^2 + 4b_1b_2 + {b_2}^2\right)}{36(b_1 + b_2)} \tag{5}$$

$$I_y = \frac{L_y(b_1 + b_2)\left({b_1}^2 + {b_2}^2\right)}{48} \tag{6}$$

2.1. **TCF under biaxial bending in each column.** There are five possible cases for a TCF subjected to an axial load and two orthogonal bending moments in each column.

Case I assumes that the entire bottom area of the footing is completely compressed. The pressures generated by the soil on the footing are obtained by means of the biaxial bending equation.

Cases II, III, IV and V assume that the entire bottom area of the footing is partially under compressed, i.e., part of the contact area is not under pressure and by integration the resultant force "R", the moment on the X axis "M_{xT}" and the moment on the Y axis "M_{yT}" are obtained. The pressures generated by the soil on the footing are estimated by means of the general equation of the pressure plane, starting from three known points.

Figure 2 shows the case I, the completely compressed area.

Figure 3 shows the cases II, III, IV and V, the partially compressed area.

The general equation of a 3-D pressure plane is

$$A_1x + A_2y + A_3\sigma_z + A_4 = 0 \tag{7}$$

where A_1, A_2, A_3 and A_4 are constants.

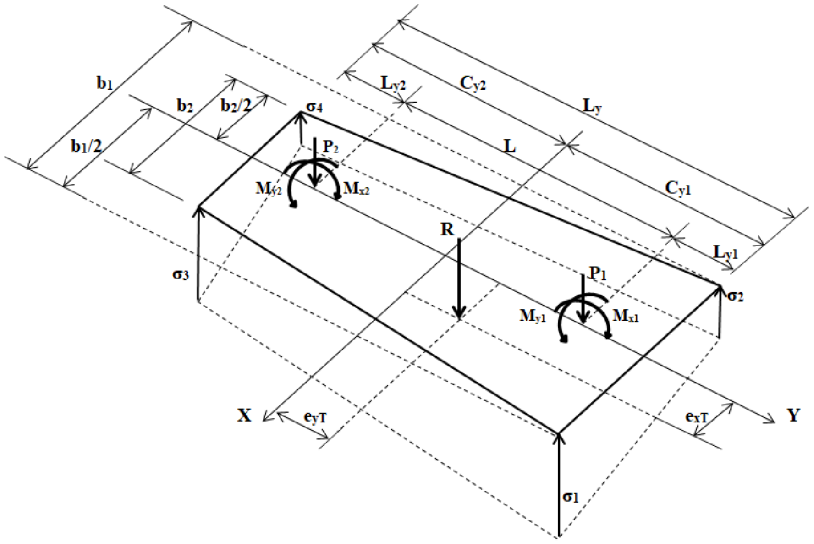

FIGURE 2. Fully compressed area

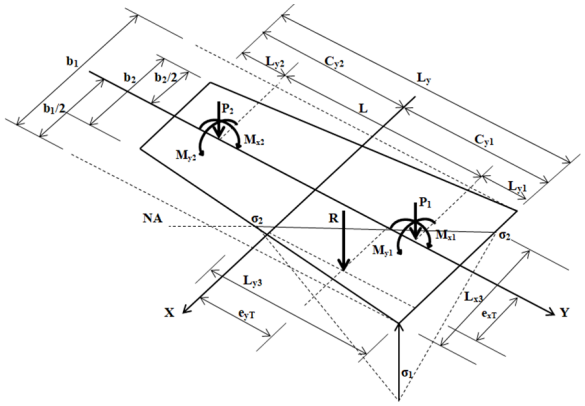

(a) Case II

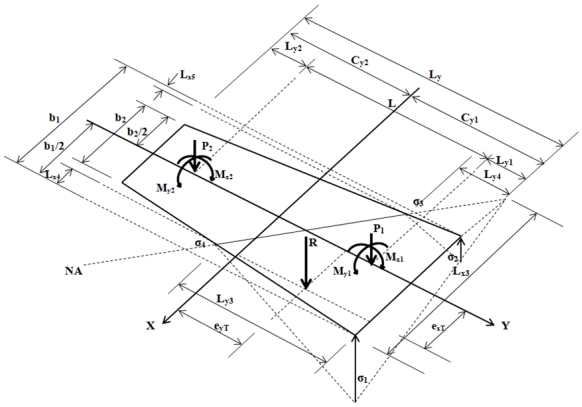

(b) Case III

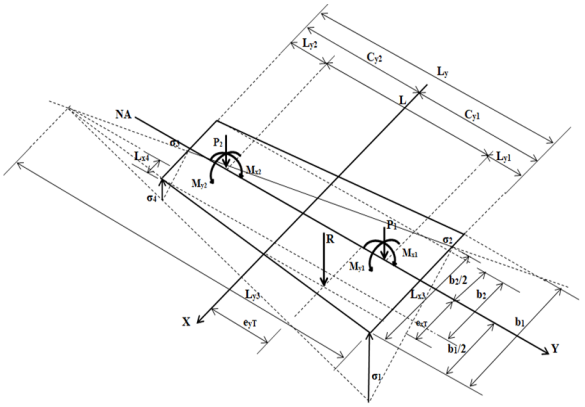

(c) Case IV

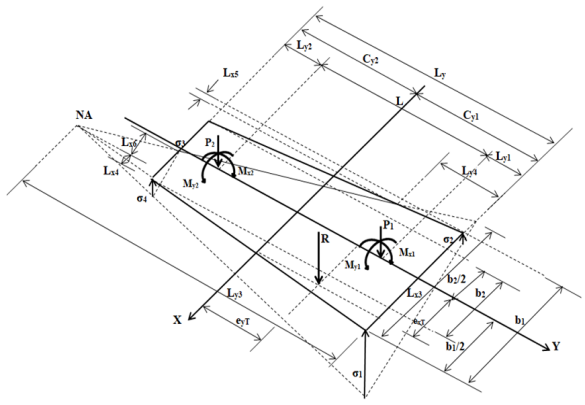

(d) Case V

FIGURE 3. Partially compressed area

For cases II, III, IV and V, the three known points of the pressure plane are

$$p_1\left(\frac{b_1}{2}, C_{y1}, \sigma_{\max}\right);\ p_2\left(\frac{b_1}{2} - L_{x3}, C_{y1}, 0\right);\ p_3\left(\frac{b_1}{2} - \frac{(b_1 - b_2)L_{y3}}{2L_y}, C_{y1} - L_{y3}, 0\right) \tag{8}$$

The general equation of the pressure plane is estimated as follows:

$$\begin{vmatrix} x-\dfrac{b_1}{2} & y-C_{y1} & \sigma_z-\sigma_{\max} \\ -L_{x3} & 0 & -\sigma_{\max} \\ -\dfrac{(b_1-b_2)L_{y3}}{2L_y} & -L_{y3} & -\sigma_{\max} \end{vmatrix} = 0 \tag{9}$$

The value of the pressure at any point σ_z is determined by solving Equation (9):

$$\sigma_z = \frac{\sigma_{\max}\{L_yL_{y3}(2x+2L_{x3}-b_1)+(y-C_{y1})[2L_yL_{x3}-(b_1-b_2)L_{y3}]\}}{2L_yL_{x3}L_{y3}} \tag{10}$$

2.1.1. *Case I.* Substituting Equations (2) to (6) in Equation (1), the soil pressures acting on the footing at each corner are determined as follows:

$$\sigma_1 = \frac{2R}{L_y(b_1+b_2)} + \frac{12M_{xT}(b_1+2b_2)}{{L_y}^2\left({b_1}^2+4b_1b_2+{b_2}^2\right)} + \frac{24M_{yT}b_1}{L_y(b_1+b_2)\left({b_1}^2+{b_2}^2\right)} \tag{11}$$

$$\sigma_2 = \frac{2R}{L_y(b_1+b_2)} + \frac{12M_{xT}(b_1+2b_2)}{{L_y}^2\left({b_1}^2+4b_1b_2+{b_2}^2\right)} - \frac{24M_{yT}b_1}{L_y(b_1+b_2)\left({b_1}^2+{b_2}^2\right)} \tag{12}$$

$$\sigma_3 = \frac{2R}{L_y(b_1+b_2)} - \frac{12M_{xT}(2b_1+b_2)}{{L_y}^2\left({b_1}^2+4b_1b_2+{b_2}^2\right)} + \frac{24M_{yT}b_2}{L_y(b_1+b_2)\left({b_1}^2+{b_2}^2\right)} \tag{13}$$

$$\sigma_4 = \frac{2R}{L_y(b_1+b_2)} - \frac{12M_{xT}(2b_1+b_2)}{{L_y}^2\left({b_1}^2+4b_1b_2+{b_2}^2\right)} - \frac{24M_{yT}b_2}{L_y(b_1+b_2)\left({b_1}^2+{b_2}^2\right)} \tag{14}$$

where

$$R = P_1 + P_2 \tag{15}$$

$$M_{xT} = M_{x1} + M_{x2} + P_1(C_{y1}-L_{y1}) - P_2(L_y - C_{y1} - L_{y2}) \tag{16}$$

$$M_{yT} = M_{y1} + M_{y2} \tag{17}$$

2.1.2. *Case II.* The general equations for R, M_{xT} and M_{yT} are determined:

$$R = \int_{C_{y1}-L_{y3}}^{C_{y1}} \int_{\frac{b_1}{2}-\left[\frac{(b_1-b_2)}{2L_y}-\frac{L_{x3}}{L_{y3}}\right](C_{y1}-y)-L_{x3}}^{\frac{b_1}{2}+\frac{(b_1-b_2)\left(C_{y1}-y\right)}{2L_y}} \sigma_z dxdy \tag{18}$$

$$R = \frac{\sigma_{\max}L_{x3}L_{y3}}{6} \tag{19}$$

$$M_{xT} = \int_{C_{y1}-L_{y3}}^{C_{y1}} \int_{\frac{b_1}{2}-\left[\frac{(b_1-b_2)}{2L_y}-\frac{L_{x3}}{L_{y3}}\right](C_{y1}-y)-L_{x3}}^{\frac{b_1}{2}+\frac{(b_1-b_2)\left(C_{y1}-y\right)}{2L_y}} \sigma_z y dxdy \tag{20}$$

$$M_{xT} = \frac{\sigma_{\max}L_{x3}L_{y3}(4C_{y1}-L_{y3})}{24} \tag{21}$$

$$M_{yT} = \int_{C_{y1}-L_{y3}}^{C_{y1}} \int_{\frac{b_1}{2}-\left[\frac{(b_1-b_2)}{2L_y}-\frac{L_{x3}}{L_{y3}}\right](C_{y1}-y)-L_{x3}}^{\frac{b_1}{2}+\frac{(b_1-b_2)\left(C_{y1}-y\right)}{2L_y}} \sigma_z x dxdy \tag{22}$$

$$M_{yT} = \frac{\sigma_{\max}L_{x3}L_{y3}[2L_y(2b_1-L_{x3})-L_{y3}(b_1-b_2)]}{48L_y} \tag{23}$$

2.1.3. *Case III.* The general equations for R, M_{xT} and M_{yT} are determined:

$$\begin{aligned}R=&\int_{\frac{b_1}{2}-\frac{(b_1-b_2)L_{y3}}{2L_y}}^{\frac{b_1}{2}}\int_{C_{y1}-\frac{(b_1-2x)L_y}{(b_1-b_2)}}^{C_{y1}}\sigma_z dydx\\&+\int_{\frac{(b_1-b_2)(L_{x3}-b_1)L_{y3}}{2\left[L_yL_{x3}-L_{y3}(b_1-b_2)\right]}-\frac{b_1}{2}}^{\frac{b_1}{2}-\frac{(b_1-b_2)L_{y3}}{2L_y}}\int_{C_{y1}-\frac{L_yL_{y3}(2L_{x3}-b_1+2x)}{2L_yL_{x3}-L_{y3}(b_1-b_2)}}^{C_{y1}}\sigma_z dydx\\&+\int_{-\frac{b_1}{2}}^{\frac{(b_1-b_2)(L_{x3}-b_1)L_{y3}}{2\left[L_yL_{x3}-L_{y3}(b_1-b_2)\right]}-\frac{b_1}{2}}\int_{C_{y1}-\frac{(b_1+2x)L_y}{(b_1-b_2)}}^{C_{y1}}\sigma_z dydx\end{aligned}\tag{24}$$

$$R=\frac{\sigma_{\max}L_{y3}}{6}\left[L_{x3}-\frac{L_y\left(L_{x3}-b_1\right)^3}{L_{x3}\left[L_yL_{x3}-L_{y3}(b_1-b_2)\right]}\right]\tag{25}$$

$$\begin{aligned}M_{xT}=&\int_{\frac{b_1}{2}-\frac{(b_1-b_2)L_{y3}}{2L_y}}^{\frac{b_1}{2}}\int_{C_{y1}-\frac{(b_1-2x)L_y}{(b_1-b_2)}}^{C_{y1}}\sigma_z ydydx\\&+\int_{\frac{(b_1-b_2)(L_{x3}-b_1)L_{y3}}{2\left[L_yL_{x3}-L_{y3}(b_1-b_2)\right]}-\frac{b_1}{2}}^{\frac{b_1}{2}-\frac{(b_1-b_2)L_{y3}}{2L_y}}\int_{C_{y1}-\frac{L_yL_{y3}(2L_{x3}-b_1+2x)}{2L_yL_{x3}-L_{y3}(b_1-b_2)}}^{C_{y1}}\sigma_z ydydx\\&+\int_{-\frac{b_1}{2}}^{\frac{(b_1-b_2)(L_{x3}-b_1)L_{y3}}{2\left[L_yL_{x3}-L_{y3}(b_1-b_2)\right]}-\frac{b_1}{2}}\int_{C_{y1}-\frac{(b_1+2x)L_y}{(b_1-b_2)}}^{C_{y1}}\sigma_z ydydx\end{aligned}\tag{26}$$

$$\begin{aligned}M_{xT}=&\frac{\sigma_{\max}L_{y3}}{24}\left[(4C_{y1}-L_{y3})L_{x3}-\frac{4C_{y1}L_y\left(L_{x3}-b_1\right)^3}{L_{x3}\left[L_yL_{x3}-L_{y3}(b_1-b_2)\right]}\right.\\&\left.+\frac{{L_y}^2L_{y3}\left(L_{x3}-b_1\right)^4}{L_{x3}\left[L_yL_{x3}-L_{y3}(b_1-b_2)\right]^2}\right]\end{aligned}\tag{27}$$

$$\begin{aligned}M_{yT}=&\int_{\frac{b_1}{2}-\frac{(b_1-b_2)L_{y3}}{2L_y}}^{\frac{b_1}{2}}\int_{C_{y1}-\frac{(b_1-2x)L_y}{(b_1-b_2)}}^{C_{y1}}\sigma_z xdydx\\&+\int_{\frac{(b_1-b_2)(L_{x3}-b_1)L_{y3}}{2\left[L_yL_{x3}-L_{y3}(b_1-b_2)\right]}-\frac{b_1}{2}}^{\frac{b_1}{2}-\frac{(b_1-b_2)L_{y3}}{2L_y}}\int_{C_{y1}-\frac{L_yL_{y3}(2L_{x3}-b_1+2x)}{2L_yL_{x3}-L_{y3}(b_1-b_2)}}^{C_{y1}}\sigma_z xdydx\\&+\int_{-\frac{b_1}{2}}^{\frac{(b_1-b_2)(L_{x3}-b_1)L_{y3}}{2\left[L_yL_{x3}-L_{y3}(b_1-b_2)\right]}-\frac{b_1}{2}}\int_{C_{y1}-\frac{(b_1+2x)L_y}{(b_1-b_2)}}^{C_{y1}}\sigma_z xdydx\end{aligned}\tag{28}$$

$$\begin{aligned}M_{yT}=&\frac{\sigma_{\max}L_{y3}}{48}\left[\frac{{b_1}^2L_y\left[L_{y3}(b_1-b_2)\left({b_1}^2+2{L_{x3}}^2\right)-2{b_1}^2L_yL_{x3}\right]}{L_{x3}\left[L_yL_{x3}-L_{y3}(b_1-b_2)\right]^2}\right.\\&\left.+\frac{4b_1L_{x3}\left[b_1L_y-L_{y3}(b_1-b_2)\right]^2}{\left[L_yL_{x3}-L_{y3}(b_1-b_2)\right]^2}-\frac{L_{x3}{L_{y3}}^3(b_1-b_2)^3}{L_y\left[L_yL_{x3}-L_{y3}(b_1-b_2)\right]^2}\right]\end{aligned}\tag{29}$$

2.1.4. *Case IV.* The general equations for R, M_{xT} and M_{yT} are determined:

$$R=\int_{C_{y1}-L_y}^{C_{y1}}\int_{\frac{b_1}{2}+\frac{\left(C_{y1}-y\right)\left[2L_{x3}L_y-(b_1-b_2)L_{y3}\right]}{2L_yL_{y3}}-L_{x3}}^{\frac{b_1}{2}-\frac{\left(C_{y1}-y\right)(b_1-b_2)}{2L_y}}\sigma_z dxdy\tag{30}$$

$$R = \frac{\sigma_{\max} L_{x3} \left[{L_{y3}}^3 - (L_{y3} - L_y)^3 \right]}{6 {L_{y3}}^2} \tag{31}$$

$$M_{xT} = \int_{C_{y1}-L_y}^{C_{y1}} \int_{\frac{b_1}{2}+\frac{\left(C_{y1}-y\right)\left[2L_{x3}L_y-(b_1-b_2)L_{y3}\right]}{2L_yL_{y3}}-L_{x3}}^{\frac{b_1}{2}-\frac{\left(C_{y1}-y\right)(b_1-b_2)}{2L_y}} \sigma_z y dx dy \tag{32}$$

$$M_{xT} = \frac{\sigma_{\max} L_y L_{x3} \left\{ 4C_{y1} \left[{L_y}^2 + 3L_{y3} \left(L_{y3} - L_y \right) \right] + L_y \left[2L_{y3} \left(4L_y - 3L_{y3} \right) - 3{L_y}^2 \right] \right\}}{24 {L_{y3}}^2} \tag{33}$$

$$M_{yT} = \int_{C_{y1}-L_y}^{C_{y1}} \int_{\frac{b_1}{2}+\frac{\left(C_{y1}-y\right)\left[2L_{x3}L_y-(b_1-b_2)L_{y3}\right]}{2L_yL_{y3}}-L_{x3}}^{\frac{b_1}{2}-\frac{\left(C_{y1}-y\right)(b_1-b_2)}{2L_y}} \sigma_z x dx dy \tag{34}$$

$$M_{yT} = \frac{\sigma_{\max} L_y L_{x3}}{48} \Bigg\{ 6(b_1 + b_2) + \frac{{L_y}^2 (b_1 + 3b_2)}{{L_{y3}}^2} + \frac{2{L_y}^2 L_{x3} \left(L_y - 4L_{y3} \right)}{{L_{y3}}^3} + \frac{4 \left[L_{x3}(3L_y - 2L_{y3}) - L_y(b_1 + 2b_2) \right]}{L_{y3}} \Bigg\} \tag{35}$$

2.1.5. *Case V.* The general equations for R, M_{xT} and M_{yT} are determined:

$$R = \int_{C_{y1}-L_y}^{C_{y1}-\frac{(L_{x3}-b_1)L_{y3}L_y}{L_yL_{x3}-(b_1-b_2)L_{y3}}} \int_{\frac{b_1}{2}+\frac{\left(C_{y1}-y\right)\left[2L_{x3}L_y-(b_1-b_2)L_{y3}\right]}{2L_yL_{y3}}}^{\frac{b_1}{2}-\frac{\left(C_{y1}-y\right)(b_1-b_2)}{2L_y}} \sigma_z dx dy + \int_{C_{y1}-\frac{(L_{x3}-b_1)L_{y3}L_y}{L_yL_{x3}-(b_1-b_2)L_{y3}}}^{C_{y1}} \int_{\frac{\left(C_{y1}-y\right)(b_1-b_2)}{2L_y}-\frac{b_1}{2}}^{\frac{b_1}{2}-\frac{\left(C_{y1}-y\right)(b_1-b_2)}{2L_y}} \sigma_z dx dy \tag{36}$$

$$R = \left[\frac{\sigma_{\max}}{6} \left\{ L_{x3}L_{y3} - \frac{\left(L_{y3} - L_y\right)^3 \left[L_y {L_{x3}}^3 - {L_{x3}}^2 L_{y3}(b_1 - b_2) + {L_{y3}}^3 L_y \right]}{{L_{x3}}{L_{y3}}^2 \left[L_y L_{x3} - L_{y3}(b_1 - b_2) \right]} \right\} \right] \tag{37}$$

$$M_{xT} = \int_{C_{y1}-L_y}^{C_{y1}-\frac{(L_{x3}-b_1)L_{y3}L_y}{L_yL_{x3}-(b_1-b_2)L_{y3}}} \int_{\frac{b_1}{2}+\frac{\left(C_{y1}-y\right)\left[2L_{x3}L_y-(b_1-b_2)L_{y3}\right]}{2L_yL_{y3}}}^{\frac{b_1}{2}-\frac{\left(C_{y1}-y\right)(b_1-b_2)}{2L_y}} \sigma_z y dx dy + \int_{C_{y1}-\frac{(L_{x3}-b_1)L_{y3}L_y}{L_yL_{x3}-(b_1-b_2)L_{y3}}}^{C_{y1}} \int_{\frac{\left(C_{y1}-y\right)(b_1-b_2)}{2L_y}-\frac{b_1}{2}}^{\frac{b_1}{2}-\frac{\left(C_{y1}-y\right)(b_1-b_2)}{2L_y}} \sigma_z y dx dy \tag{38}$$

$$M_{xT} = \frac{\sigma_{\max}}{24} \Bigg[L_{x3}L_{y3} \left(4C_{y1} - L_{y3} \right) - \frac{\left(L_{y3} - L_y\right)^3 L_{x3} \left(4C_{y1} - 3L_y - L_{y3} \right)}{{L_{y3}}^2} - \frac{4C_{y1} \left(L_{x3} - b_1 \right)^3 L_{y3} L_y}{L_{x3} \left[L_y L_{x3} - L_{y3}(b_1 - b_2) \right]} + \frac{\left(L_{x3} - b_1 \right)^4 {L_{y3}}^2 {L_y}^2}{L_{x3} \left[L_y L_{x3} - L_{y3}(b_1 - b_2) \right]^2} \Bigg] \tag{39}$$

$$M_{yT} = \int_{C_{y1}-L_y}^{C_{y1}-\frac{(L_{x3}-b_1)L_{y3}L_y}{L_yL_{x3}-(b_1-b_2)L_{y3}}} \int_{\frac{b_1}{2}+\frac{\left(C_{y1}-y\right)\left[2L_{x3}L_y-(b_1-b_2)L_{y3}\right]}{2L_yL_{y3}}}^{\frac{b_1}{2}-\frac{\left(C_{y1}-y\right)(b_1-b_2)}{2L_y}} \sigma_z x dx dy + \int_{C_{y1}-\frac{(L_{x3}-b_1)L_{y3}L_y}{L_yL_{x3}-(b_1-b_2)L_{y3}}}^{C_{y1}} \int_{\frac{\left(C_{y1}-y\right)(b_1-b_2)}{2L_y}-\frac{b_1}{2}}^{\frac{b_1}{2}-\frac{\left(C_{y1}-y\right)(b_1-b_2)}{2L_y}} \sigma_z x dx dy \tag{40}$$

$$M_{yT} = \frac{\sigma_{\max}}{24}\left[L_{x3}L_{y3}(4C_{y1} - L_{y3}) - \frac{(L_{y3} - L_y)^3 L_{x3}(4C_{y1} - 3L_y - L_{y3})}{{L_{y3}}^2} - \frac{4C_{y1}(L_{x3} - b_1)^3 L_{y3}L_y}{L_{x3}[L_yL_{x3} - L_{y3}(b_1 - b_2)]} + \frac{(L_{x3} - b_1)^4 {L_{y3}}^2 {L_y}^2}{L_{x3}[L_yL_{x3} - L_{y3}(b_1 - b_2)]^2}\right] \tag{41}$$

2.2. **TCF under uniaxial bending in each column.** There are four possible cases for a TCF subjected to an axial load and a bending moment at each column (moments in the same direction).

Cases I-X and I-Y assume that the entire bottom area of the footing is completely compressed.

Cases II-X and II-Y assume that the entire bottom area of the footing is partially compressed.

For cases I-X and II-X, the equation presented in Section 2.1 (TCF under biaxial bending in each column) is used, but $M_{x1} = 0$ and $M_{x2} = 0$.

For case I-Y, Equations (11) to (17) are used, but $M_{yT} = 0$ because $M_{y1} = 0$ and $M_{y2} = 0$.

Case II-Y. Figure 4 represents case II-Y, the entire area of the footing is partially compressed.

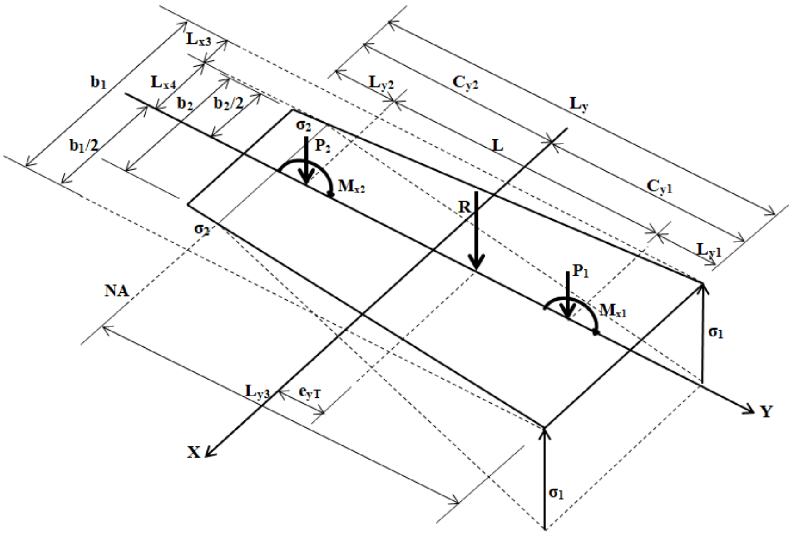

FIGURE 4. Case II-Y

Now, for case II-Y, the three known points of the pressure plane are

$$p_1\left(\frac{b_1}{2}, C_{y1}, \sigma_{\max}\right);\ p_2\left(-\frac{b_1}{2}, C_{y1}, \sigma_{\max}\right);\ p_3\left(\frac{L_yb_1 - (b_1 - b_2)L_{y3}}{2L_y}, C_{y1} - L_{y3}, 0\right) \tag{42}$$

The general equation of the pressure plane is determined as follows:

$$\begin{vmatrix} x - \frac{b_1}{2} & y - C_{y1} & \sigma_z - \sigma_{\max} \\ -b_1 & 0 & 0 \\ -\frac{(b_1 - b_2)L_{y3}}{2L_y} & -L_{y3} & -\sigma_{\max} \end{vmatrix} = 0 \tag{43}$$

The pressure σ_z at any point of the footing is determined by solving Equation (43):

$$\sigma_z = \frac{\sigma_{\max}(L_{y3} - C_{y1} + y)}{L_{y3}} \tag{44}$$

The equations for R and M_{xT} are determined:

$$R = 2\int_{C_{y1}-L_{y3}}^{C_{y1}} \int_{0}^{\frac{b_1}{2} - \frac{(b_1-b_2)\left(C_{y1}-y\right)}{2L_y}} \sigma_z dx dy \tag{45}$$

$$R = \frac{\sigma_{\max} L_{y3}\left[3b_1 L_y - (b_1 - b_2)L_{y3}\right]}{6L_y} \tag{46}$$

$$M_{xT} = 2\int_{C_{y1}-L_{y3}}^{C_{y1}} \int_{0}^{\frac{b_1}{2} - \frac{(b_1-b_2)\left(C_{y1}-y\right)}{2L_y}} \sigma_z y dx dy \tag{47}$$

$$M_{xT} = \frac{\sigma_{\max} L_{y3}\left[2L_y b_1\left(3C_{y1} - L_{y3}\right) - L_{y3}(b_1 - b_2)\left(2C_{y1} - L_{y3}\right)\right]}{12L_y} \tag{48}$$

2.3. **Minimum area for TCFs.** Minimum area (objective) for any case is

$$A_{\min} = \frac{L_y(b_1 + b_2)}{2} \tag{49}$$

The constraints for biaxial bending in each case are indicated in Table 1.

Table 1. Constraints for biaxial bending

Case	Equations of the constraints
I	$0 \leq$ Equations (11) to (14), Equations (11) to (14) $\leq \sigma_{\max}$, Equations (15) to (17), $L_y = L_{y1} + L + L_{y2}$
II	Equation (15) $\leq$ Equation (19), Equation (16) $\leq$ Equation (21), Equation (17) $\leq$ Equation (23), $L_y = L_{y1} + L + L_{y2}$, $b_1 \geq L_{x3}$, $L_y \geq L_{y3}$
III	Equation (15) $\leq$ Equation (25), Equation (16) $\leq$ Equation (27), Equation (17) $\leq$ Equation (29), $L_y = L_{y1} + L + L_{y2}$, $b_1 \leq L_{x3}$, $L_y \geq L_{y3}$
IV	Equation (15) $\leq$ Equation (31), Equation (16) $\leq$ Equation (33), Equation (17) $\leq$ Equation (35), $L_y = L_{y1} + L + L_{y2}$, $b_1 \geq L_{x3}$, $L_y \leq L_{y3}$
V	Equation (15) $\leq$ Equation (37), Equation (16) $\leq$ Equation (39), Equation (17) $\leq$ Equation (41), $L_y = L_{y1} + L + L_{y2}$, $b_1 \leq L_{x3}$, $L_y \leq L_{y3}$

Note: $b_1 \geq c_{x1}$, $b_2 \geq c_{x2}$, $L_{y1} \geq c_{y1}$ and $L_{y2} \geq c_{y2}$.

The constraints that can be limited in the Y-axis direction are

1) Not limited: $L_{y1} \geq c_{y1}/2$ and $L_{y2} \geq c_{y2}/2$ (Columns 1 and 2 can take any position at the base of the footing); 2) Limited in column 1: $L_{y1} = c_{y1}/2$ and $L_{y2} \geq c_{y2}/2$ (Column 1 is located at the edge of the footing base); 3) Limited in column 2: $L_{y1} \geq c_{y1}/2$ and $L_{y2} = c_{y2}/2$ (Column 2 is located at the edge of the footing base); 4) Limited in both columns: $L_{y1} = c_{y1}/2$ and $L_{y2} = c_{y2}/2$ (Columns 1 and 2 are located at the edges of the footing base).

The constraints for uniaxial bending in each case are presented in Table 2.

Figure 5 represents the flowchart using the equations proposed and how to use Maple software to determine the minimum area for a TCF.

3. **Numerical Studies.** Two numerical studies are shown to find the minimum area of TCFs subjected to biaxial bending for the five cases and each study is presented for the four types of constraints in the Y-axis direction (unconstrained, constrained in column 1, constrained in column 2, constrained in columns 1 and 2). Study 1: $P_1 = 250$, 500, 750,

TABLE 2. Constraints for uniaxial bending

Case	Equations of the constraints
I-X	$0 \leq$ Equations (11) to (14), Equations (11) to (14) $\leq \sigma_{\max}$, Equations (15) to (17), $M_{x1} = 0$, $M_{x2} = 0$, $L_y = L_{y1} + L + L_{y2}$
II-X	Equations of the five cases described in Table 1
I-Y	$0 \leq$ Equations (11) to (14), Equations (11) to (14) $\leq \sigma_{\max}$, Equations (15) to (17), $M_{y1} = 0$, $M_{y2} = 0$, $L_y = L_{y1} + L + L_{y2}$
II-Y	Equation (15) $\leq$ Equation (46), Equation (16) $\leq$ Equation (48), $L_y = L_{y1} + L + L_{y2}$

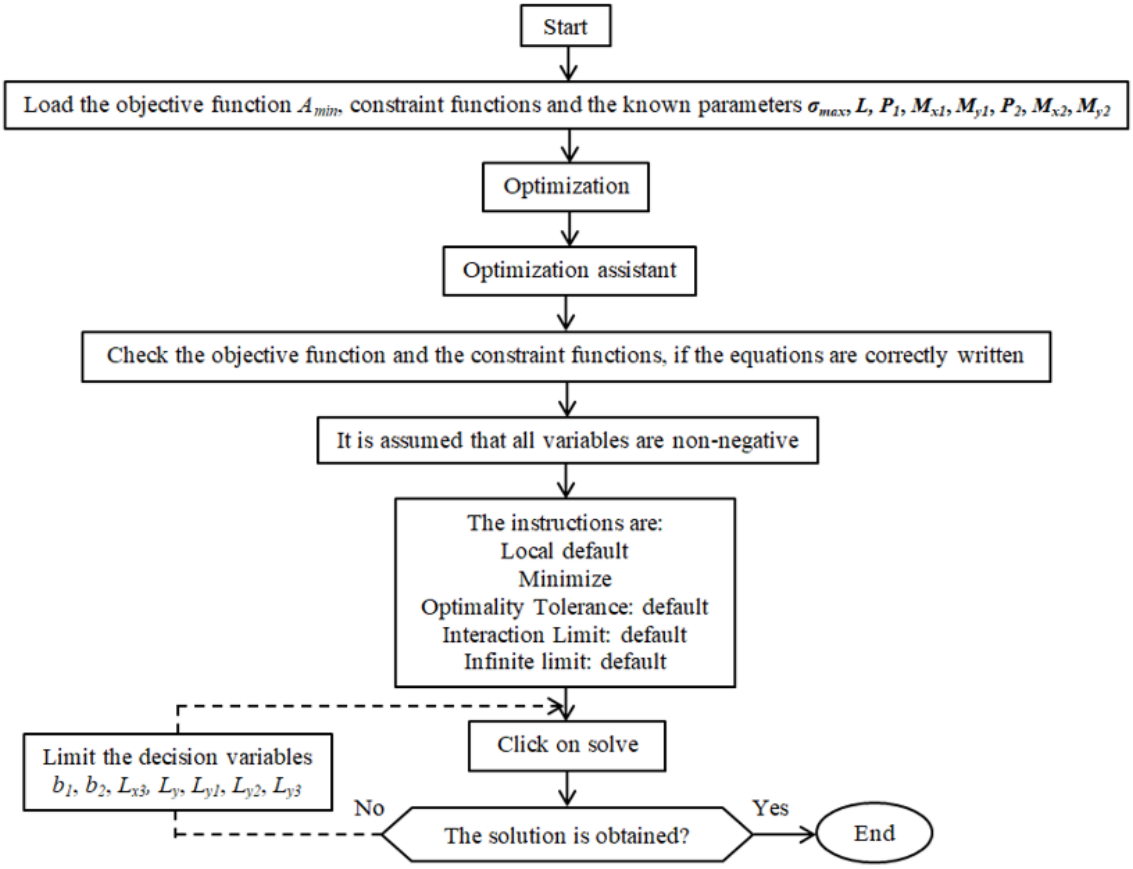

FIGURE 5. Flowchart for a trapezoidal combined footing

1000 kN; $M_{x1} = M_{y1} = 250$ kN-m; $P_2 = 500$ kN; $M_{x2} = M_{y2} = 500$ kN-m; $L = 5.00$ m; $\sigma_{\max} = 200$ kN/m^2. Study 2: The same values of study 1, but $L = 7.00$ m. For all studies it is limited to b_1 and $b_2 \geq 0.40$ (see Tables 3 to 6).

Two numerical studies are presented to estimate the minimum area of TCFs subjected to uniaxial bending due to each column ($M_{x1} = M_{x2} = 0$ kN-m) for the five cases. Study 1: $P_1 = 250$, 500, 750, 1000 kN; $M_{x1} = 0$ kN-m; $M_{y1} = 250$ kN-m; $P_2 = 500$ kN; $M_{x2} = 0$ kN-m; $M_{y2} = 500$ kN-m; $L = 5.00$ m; $\sigma_{\max} = 200$ kN/m^2. Study 2: The same values of study 1, but $L = 7.00$ m. For all studies it is limited to b_1 and $b_2 \geq 0.40$ (see Table 7).

Four numerical studies are shown to estimate the minimum area for TCFs subjected to uniaxial bending due to each column ($M_{y1} = M_{y2} = 0$ kN-m) for the two cases (resultant force is on the Y axis). Study 1: $P_1 = 250$, 500, 750, 1000 kN; $M_{x1} = 250$ kN-m; $M_{y1} = 0$ kN-m; $P_2 = 500$ kN; $M_{x2} = 500$ kN-m; $M_{y2} = 0$ kN-m; $L = 5.00$ m; $\sigma_{\max} = 200$ kN/m^2.

TABLE 3. Biaxial bending (unconstrained sides)

L (m)	P_1 (kN)	Case	b_1 (m)	b_2 (m)	L_y (m)	L_{x3} (m)	L_{y1} (m)	L_{y2} (m)	L_{y3} (m)	$A_{\min}$ (m^2)
Study 1										
5.00	250	IV	5.33	0.40	5.40	1.65	0.20	0.20	31.78	15.46
	500	IV	5.06	0.40	5.40	3.62	0.20	0.20	8.78	14.75
	750	IV	4.94	0.40	6.00	3.98	0.80	0.20	10.08	16.03
	1000	I	5.24	0.40	6.04	–	0.84	0.20	–	17.06
Study 2										
7.00	250	V	0.40	4.84	7.62	1.00	0.20	0.42	4084.93	19.98
	500	IV	4.26	0.40	7.40	2.26	0.20	0.20	15.48	17.23
	750	IV	4.34	0.40	7.57	3.53	0.37	0.20	10.96	17.91
	1000	IV	4.10	0.40	8.54	3.29	1.34	0.20	14.78	19.21

TABLE 4. Biaxial bending (constrained side in column 1)

L (m)	P_1 (kN)	Case	b_1 (m)	b_2 (m)	L_y (m)	L_{x3} (m)	L_{y1} (m)	L_{y2} (m)	L_{y3} (m)	$A_{\min}$ (m^2)
Study 1										
5.00	250	IV	5.33	0.40	5.40	1.65	0.20	0.20	31.78	15.46
	500	IV	5.06	0.40	5.40	3.62	0.20	0.20	8.78	14.75
	750	I	5.64	0.40	5.40	–	0.20	0.20	–	16.30
	1000	V	6.51	0.40	5.40	8.83	0.20	0.20	5.42	18.66
Study 2										
7.00	250	V	0.40	4.84	7.62	1.00	0.20	0.42	4084.93	19.98
	500	IV	4.26	0.40	7.40	2.26	0.20	0.20	15.48	17.23
	750	IV	4.45	0.40	7.40	3.82	0.20	0.20	10.00	17.93
	1000	I-V	5.00	0.40	7.40	5.58	0.20	0.20	8.17	19.98

TABLE 5. Biaxial bending (constrained side in column 2)

L (m)	P_1 (kN)	Case	b_1 (m)	b_2 (m)	L_y (m)	L_{x3} (m)	L_{y1} (m)	L_{y2} (m)	L_{y3} (m)	$A_{\min}$ (m^2)
Study 1										
5.00	250	IV	5.33	0.40	5.40	1.65	0.20	0.20	31.78	15.46
	500	IV	5.06	0.40	5.40	3.62	0.20	0.20	8.78	14.75
	750	IV	4.94	0.40	6.00	3.98	0.80	0.20	10.08	16.03
	1000	I	5.24	0.40	6.04	–	0.84	0.20	–	17.06
Study 2										
7.00	250	V	0.51	3.82	7.40	0.55	0.20	0.20	411105.44	16.02
	500	IV	4.26	0.40	7.40	2.26	0.20	0.20	15.48	17.23
	750	IV	3.67	0.40	9.98	1.26	2.78	0.20	1836.36	20.30
	1000	IV	4.10	0.40	8.54	3.29	1.34	0.20	14.78	19.21

Study 2: The same values of study 1, but $L = 7.00$ m. Study 3: $P_1 = 250$, 500, 750, 1000 kN; $M_{x1} = 2250$ kN-m; $M_{y1} = 0$ kN-m; $P_2 = 500$ kN; $M_{x2} = 2500$ kN-m; $M_{y2} = 0$ kN-m; $L = 5.00$ m; $\sigma_{\max} = 200$ kN/m^2. Study 4: The same values of study 3, but $L = 7.00$ m. For studies 1 and 2 it is limited to b_1 and $b_2 \geq 0.40$ (see Table 8) and for studies 3 and 4 it is limited to b_1 and $b_2 \geq 1.00$ (see Table 9).

TABLE 6. Biaxial bending (constrained sides in columns 1 and 2)

L (m)	P_1 (kN)	Case	b_1 (m)	b_2 (m)	L_y (m)	L_{x3} (m)	L_{y1} (m)	L_{y2} (m)	L_{y3} (m)	$A_{\min}$ (m^2)
Study 1										
5.00	250	IV	5.33	0.40	5.40	1.65	0.20	0.20	31.78	15.46
	500	IV	5.06	0.40	5.40	3.62	0.20	0.20	8.78	14.75
	750	I	5.64	0.40	5.40	–	0.20	0.20	–	16.30
	1000	III	6.51	0.40	5.40	8.83	0.20	0.20	5.42	18.66
Study 2										
7.00	250	V	0.51	3.82	7.40	0.55	0.20	0.20	411105.44	16.02
	500	IV	4.26	0.40	7.40	2.26	0.20	0.20	15.48	17.23
	750	IV	4.45	0.40	7.40	3.82	0.20	0.20	10.00	17.93
	1000	I-V	5.00	0.40	7.40	5.58	0.20	0.20	8.17	19.98

TABLE 7. Uniaxial bending for $M_{x1} = M_{x2} = 0$ kN-m (unconstrained sides)

L (m)	P_1 (kN)	Case	b_1 (m)	b_2 (m)	L_y (m)	L_{x3} (m)	L_{y1} (m)	L_{y2} (m)	L_{y3} (m)	$A_{\min}$ (m^2)
Study 1										
5.00	250	V	0.40	4.96	6.94	1.11	0.20	1.74	1483.90	18.59
	500	V	0.40	4.69	5.75	1.90	0.55	0.20	517.09	14.64
	750	IV	5.18	0.40	5.40	3.72	0.20	0.20	12.16	15.07
	1000	IV	5.09	0.40	6.02	3.90	0.82	0.20	14.30	16.52
Study 2										
7.00	250	V	0.40	4.61	9.67	0.78	0.20	2.47	4387.61	24.21
	500	V	0.41	4.20	7.67	1.37	0.47	0.20	1018.17	17.69
	750	IV	4.26	0.40	7.40	2.74	0.20	0.20	16.38	17.23
	1000	IV	4.30	0.40	7.87	3.43	0.67	0.20	14.50	18.50

TABLE 8. Uniaxial bending for $M_{y1} = M_{y2} = 0$ kN-m and $b_1 = b_2 \geq 0.40$ m (unconstrained sides)

L (m)	P_1 (kN)	Case	b_1 (m)	b_2 (m)	L_y (m)	L_{y1} (m)	L_{y2} (m)	L_{y3} (m)	$A_{\min}$ (m^2)
Study 1									
5.00	250	I-Y	0.40	0.74	6.58	1.28	0.30	–	3.75
	500	I-Y	1.26	0.40	6.04	0.75	0.29	–	5.00
	750	I-Y	1.54	0.40	6.44	1.19	0.25	–	6.25
	1000	I-Y	1.82	0.40	6.74	1.48	0.26	–	7.50
Study 2									
7.00	250	I-Y	0.40	0.56	7.77	0.44	0.33	–	3.75
	500	I-Y	0.83	0.40	8.16	0.86	0.30	–	5.00
	750	I-Y	0.63	0.45	11.60	3.28	1.32	–	6.25
	1000	I-Y	1.19	0.40	9.44	2.11	0.33	–	7.50

Only studies that generate the smallest minimum area for each study are presented.

TABLE 9. Uniaxial bending for $M_{y1} = M_{y2} = 0$ kN-m and $b_1 = b_2 \geq 1.00$ m (unconstrained sides)

L (m)	P_1 (kN)	Case	b_1 (m)	b_2 (m)	L_y (m)	L_{y1} (m)	L_{y2} (m)	L_{y3} (m)	$A_{\min}$ (m^2)
Study 3									
5.00	250	II-Y	1.00	1.00	10.70	5.50	0.20	7.50	10.70
	500	II-Y	1.00	1.00	10.78	5.58	0.20	10.00	10.78
	750	I-Y	1.00	1.00	11.12	5.92	0.20	–	11.12
	1000	I-Y	1.00	1.00	11.41	6.21	0.20	–	11.41
Study 4									
7.00	250	II-Y	1.00	1.00	11.37	4.17	0.20	7.50	11.37
	500	II-Y	1.00	1.00	11.78	4.58	0.20	10.00	11.78
	750	I-Y	1.00	1.00	12.37	5.17	0.20	–	12.37
	1000	I-Y	1.00	1.00	12.94	5.74	0.20	–	12.94

4. **Results.** One way to verify the equations for TCFs subjected to biaxial bending for cases II, III, IV and V is as follows:

Case II as seen in Figure 3(a):

1.- Substituting $x = b_1/2$ and $y = C_{y1}$ into Equation (10), $\sigma_1 = \sigma_{\max}$ is obtained.

2.- Substituting $x = b_1/2 - L_{x3}$ and $y = C_{y1}$ into Equation (10), $\sigma_2 = 0$ is determined.

3.- Substituting $x = b_1/2 - (b_1 - b_2)L_{y3}/2L_y$ and $y = C_{y1} - L_{y3}$ into Equation (10), $\sigma_3 = 0$ is obtained.

Case III as seen in Figure 3(b):

1.- Substituting $x = b_1/2$ and $y = C_{y1}$ into Equation (10), $\sigma_1 = \sigma_{\max}$ is obtained.

2.- Substituting $x = -b_1/2$ and $y = C_{y1}$ into Equation (10), $\sigma_2 = \sigma_{\max}(L_{x3} - b_1)/L_{x3}$ is determined. Also, it can be verified by proportions.

3.- Substituting $x = b_1/2 - (b_1 - b_2)L_{y3}/2L_y$ and $y = C_{y1} - L_{y4}$ into Equation (10), $\sigma_3 = 0$ is obtained. Where $L_{y4} = (L_{x3} - b_1)L_yL_{y3}/[L_yL_{y3} - L_{y3}(b_1 - b_2)]$.

4.- Substituting $x = b_1/2 - L_{x4}$ and $y = C_{y1} - L_{y3}$ into Equation (10), $\sigma_4 = 0$ is determined. Where $L_{x4} = (b_1 - b_2)L_{y3}/2L_y$.

Case IV as seen in Figure 3(c):

1.- Substituting $x = b_1/2$ and $y = C_{y1}$ into Equation (10), $\sigma_1 = \sigma_{\max}$ is obtained.

2.- Substituting $x = b_1/2 - L_{x3}$ and $y = C_{y1}$ into Equation (10), $\sigma_2 = 0$ is determined.

3.- Substituting $x = b_2/2 - (L_{y3} - L_y)L_{x3}/L_{y3}$ and $y = C_{y1} - L_y$ into Equation (10), $\sigma_3 = 0$ is obtained.

4.- Substituting $x = b_2/2$ and $y = C_{y1} - L_y$ into Equation (10), $\sigma_4 = \sigma_{\max}(L_{y3} - L_y)/L_{y3}$ is determined. Also, it can be verified by proportions.

Case V as seen in Figure 3(d):

1.- Substituting $x = b_1/2$ and $y = C_{y1}$ into Equation (10), $\sigma_1 = \sigma_{\max}$ is obtained.

2.- Substituting $x = -b_1/2$ and $y = C_{y1}$ into Equation (10), $\sigma_2 = \sigma_{\max}(L_{x3} - b_1)/L_{x3}$ is determined. Also, it can be verified by proportions.

3.- Substituting $x = b_2/2 - (L_{y3} - L_y)L_{x3}/L_{y3}$ and $y = C_{y1} - L_y$ into Equation (10), $\sigma_3 = 0$ is obtained.

4.- Substituting $x = b_2/2$ and $y = C_{y1} - L_y$ into Equation (10), $\sigma_4 = \sigma_{\max}(L_{y3} - L_y)/L_{y3}$ is determined. Also, it can be verified by proportions.

One way to verify the equation for TCFs subjected to uniaxial bending for the case II-Y is as follows (see Figure 4):

1.- Substituting $y = C_{y1}$ into Equation (44), $\sigma_1 = \sigma_{\max}$ is obtained.

2.- Substituting $y = C_{y1} - L_{y3}$ in Equation (44), $\sigma_2 = 0$ is determined.

Another way to verify the equations for TCFs subjected to biaxial bending for cases I, II, III, IV and V is as follows:

1.- By substituting b_1 and $b_2 = L_x$ into Equations (11) to (14), Equations (7) to (10) are obtained for rectangular combined footings [29].

2.- By substituting C_{y1}, and setting b_1 and $b_2 = L_x$ into Equations (19), (21) and (23), Equations (24) to (26) are obtained for rectangular combined footings [29].

3.- By substituting C_{y1}, and setting b_1 and $b_2 = L_x$ into Equations (25), (27) and (29), Equations (20) to (22) are obtained for rectangular combined footings [29].

4.- By substituting C_{y1}, and setting b_1 and $b_2 = L_x$ into Equations (31), (33) and (35), Equations (16) to (18) are obtained for rectangular combined footings [29].

5.- By substituting C_{y1}, and setting b_1 and $b_2 = L_x$ into Equations (37), (39) and (41), Equations (12) to (14) are obtained for rectangular combined footings [29].

The results of minimum areas for TCFs subjected to biaxial bending are shown in Tables 3, 4, 5 and 6 which present the following.

Table 3 (unconstrained sides) shows the following: Study 1, the first three appear in case IV and the last in case I. When P_1 increases: L_y and L_{y1} are the same up to $P_1 =$ 500 kN and then increase; L_{y2} and b_2 are the same; b_1 decreases up to $P_1 = 750$ kN and then increases; $A_{\min}$ decreases up to $P_1 = 500$ kN and then increases. Study 2, the first appears in case V and the last three appear in case IV. When P_1 increases: L_y and $A_{\min}$ decrease up to $P_1 = 500$ kN and then increase; L_{y2} and b_2 decrease until $P_1 = 500$ kN and then are equal; L_{y1} is the same until $P_1 = 500$ kN and then increases; b_1 increases until $P_1 = 750$ kN and then decreases.

Table 4 (constrained side in column 1) presents the following: Study 1, the first two appear in case IV, third appears in case I and the last in case V. When P_1 increases: L_y, b_2, L_{y1} and L_{y2} are the same; b_1 and $A_{\min}$ decrease up to $P_1 = 500$ kN and then increase. Study 2, the first appears in case V, the second and third in case IV and the last in cases I and V. When P_1 increases: L_y, L_{y2} and b_2 decrease until $P_1 = 500$ kN and then are equal; L_{y1} is the same; b_1 increases; $A_{\min}$ decreases up to $P_1 = 500$ kN and then increases.

Table 5 (constrained side in column 2) shows the following: Study 1 shows the same results as Table 3 in study 1. Study 2, the first appears in case V and the last three appear in case IV. When P_1 increases: L_y and L_{y1} are the same up to $P_1 = 500$ kN, then increase up to $P_1 = 750$ kN and subsequently decrease; L_{y2} is the same; b_1 increases up to $P_1 =$ 500 kN, then decreases up to $P_1 = 750$ kN and subsequently increases; b_2 decreases up to $P_1 = 500$ kN, and then is equal; $A_{\min}$ increases up to $P_1 = 750$ kN and then decreases.

Table 6 (constrained sides in columns 1 and 2) presents the following: Study 1 shows the same results as Table 4 in study 1. Study 2, the first appears in case V, the second and third in case IV and the last in cases I and V. When P_1 increases: L_y, L_{y1} and L_{y2} are the same; b_1 and $A_{\min}$ increase; b_2 decreases until $P_1 = 500$ kN and then is equal.

The results of minimum areas for trapezoidal combined footings subjected to uniaxial bending are presented in Tables 7 to 9 which show the following.

Table 7 (unconstrained sides) shows the following: Study 1, the first two appear in case V and the two last appear in case IV. When P_1 increases: b_1 is the same up to $P_1 = 500$ kN, then increases up to $P_1 = 750$ kN and subsequently decreases; b_2 decreases up to $P_1 = 750$ kN and then is the same; L_y decreases up to $P_1 = 750$ kN, and then increases; L_{y1} increases up to $P_1 = 500$ kN, then decreases up to $P_1 = 750$ kN and subsequently increases; L_{y2} decreases up to $P_1 = 500$ kN and then is equal; $A_{\min}$ decreases up to $P_1 =$ 500 kN and then increases. Study 2, the first two appear in case V and the two last appear in case IV. When P_1 increases: b_1 increases; b_2 decreases up to $P_1 = 750$ kN and then is the same; L_y decreases up to $P_1 = 750$ kN and then increases; L_{y1} increases up to $P_1 =$

500 kN, then decreases up to $P_1 = 750$ kN and subsequently increases; L_{y2} decreases up to $P_1 = 500$ kN and then is equal; $A_{\min}$ decreases up to $P_1 = 750$ kN and then increases.

Table 8 (unconstrained sides) presents the following: Study 1, all appear in case I-Y. When P_1 increases: b_1 increases; b_2 decreases up to $P_1 = 500$ kN and then is the same; L_y and L_{y1} decrease up to $P_1 = 500$ kN and then increase; L_{y2} decreases up to $P_1 = 750$ kN and then increases; $A_{\min}$ increases. Study 2, all appear in case I-Y. When P_1 increases: b_1 increases up to $P_1 = 500$ kN, then decreases up to $P_1 = 750$ kN and subsequently increases; b_2 decreases up to $P_1 = 500$ kN and then increases up to $P_1 = 750$ kN and subsequently decreases; L_y and L_{y1} increase up to $P_1 = 750$ kN and then decrease; L_{y2} decreases up to $P_1 = 500$ kN, then increases up to $P_1 = 750$ kN and subsequently decreases; $A_{\min}$ increases.

The minimum area depends first on L_{y1}, L_{y2}, b_1 and b_2, but a generalized trend cannot be presented because they appear in different cases.

Table 9 (unconstrained sides) shows the following: Study 1, the first two appear in case II-Y and the two last appear in case I-Y. When P_1 increases: L_y and L_{y1} increase; b_1, b_2 and L_{y2} are the same; $A_{\min}$ increases. Study 2 shows the same behavior as study 1.

Figure 6 shows the minimum areas of the CM (current model) or case I (values at the top) and NM (new model) or cases II, III, IV and V (values at the bottom) for biaxial bending.

Figure 7 shows the minimum areas of the CM or case I and NM or cases II, III, IV and V for uniaxial bending with $M_{x1} = M_{x2} = 0$ kN-m (unconstrained sides).

Figure 8 shows the minimum areas of the CM or case I-Y and NM or cases II-Y for uniaxial bending (unconstrained sides) with $M_{y1} = M_{y2} = 0$ kN-m with $b_1 = b_2 \geq 0.40$ m for studies 1 and 2, and with $b_1 = b_2 \geq 1.00$ m for studies 3 and 4.

Figure 6(a) (Unconstrained sides) shows the following: The CM is greater than the NM in all cases except in study 1 for $P_1 = 1000$ kN. The biggest difference occurs at $P_1 = 250$ kN for study 1 of 2.08 times, and for study 2 of 2.22 times. The minor difference occurs at $P_1 = 1000$ kN for study 1 of 0.99 times, and for study 2 of 1.01 times.

Figure 6(b) (Constrained side in column 1) presents the following: The CM is greater than the NM in all cases except in study 1 for $P_1 = 750$ kN. The biggest difference occurs at $P_1 = 1000$ kN for study 1 of 2.88 times, and at $P_1 = 250$ kN for study 2 of 2.22 times. The minor difference occurs at $P_1 = 750$ kN for study 1 of 0.96 times, and for study 2 occurs at $P_1 = 1000$ kN of 0 times.

Figure 6(c) (Constrained side in column 2) shows the following: The CM is greater than the NM in all cases except in study 1 for $P_1 = 1000$ kN. The biggest difference occurs at $P_1 = 250$ kN for study 1 of 2.08 times, and for study 2 of 2.76 times. The minor difference occurs at $P_1 = 1000$ kN for study 1 of 0.99 times, and for study 2 of 1.01 times.

Figure 6(d) (Constrained sides in columns 1 and 2) presents the following: The CM is greater than the NM in all cases except in study 1 for $P_1 = 750$ kN. The biggest difference occurs at $P_1 = 1000$ kN for study 1 of 2.88 times, and at $P_1 = 250$ kN for study 2 of 2.76 times. The minor difference occurs at $P_1 = 750$ kN for study 1 of 0.96 times, and for study 2 occurs at $P_1 = 1000$ kN of 0 times.

Figure 7 shows the following: The CM is greater than the NM in all cases. The biggest difference occurs at $P_1 = 500$ kN for study 1 of 1.66 times, and for study 2 of 1.88 times. The minor difference occurs at $P_1 = 1000$ kN for study 1 of 1.09 times and for study 2 of 1.07 times.

Figure 8(a) presents the following: The NM is greater than the CM in all cases. The biggest difference occurs at $P_1 = 250$ kN for study 1 of 1.73 times, and for study 2 of 1.90 times.

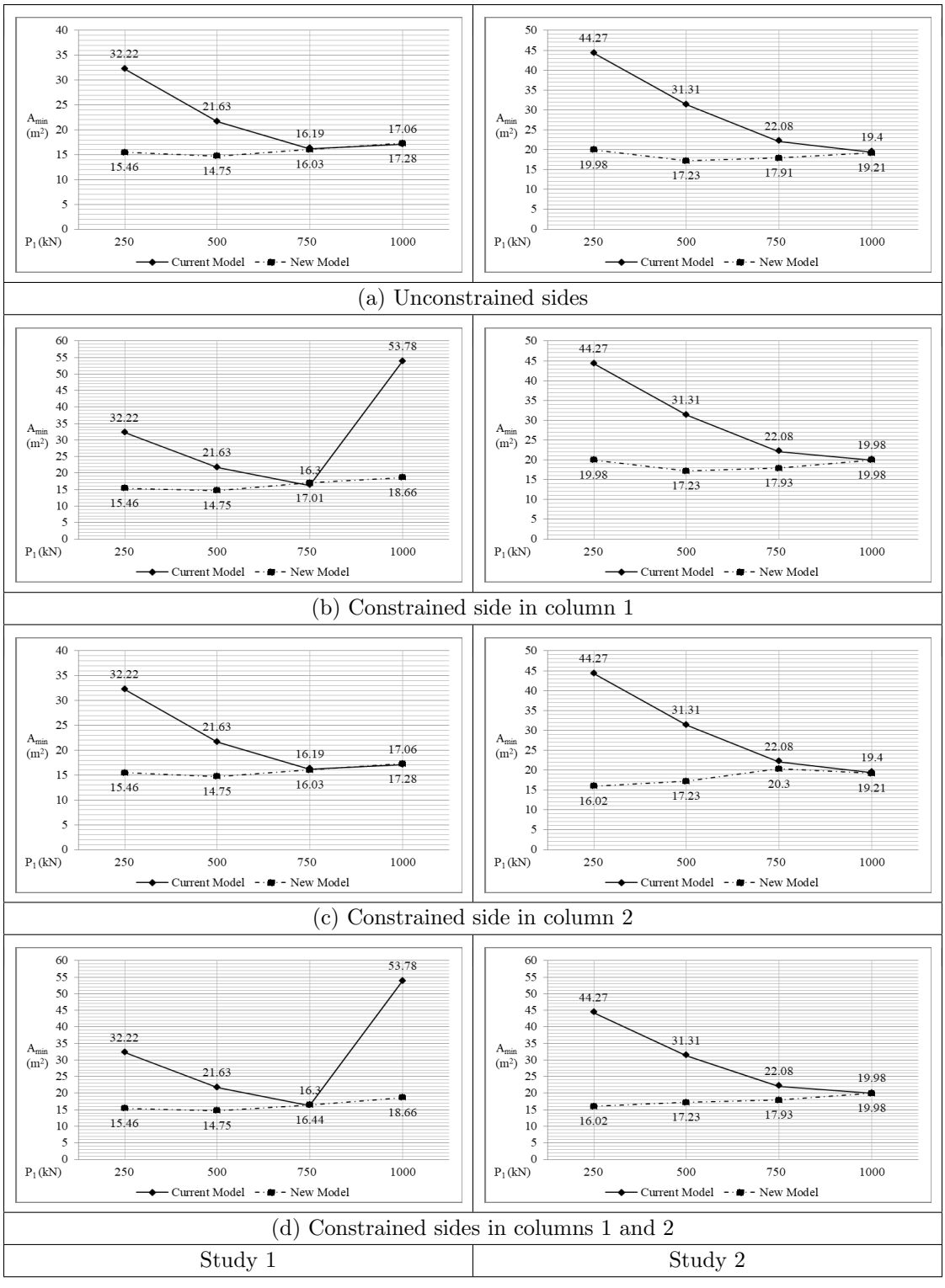

FIGURE 6. Comparison of minimum areas for biaxial bending of the two models

Figure 8(b) shows the following: The CM is larger than the NM in the first two cases and the NM is larger in the last two cases for both studies. The greatest difference is given at $P_1 = 250$ kN for study 3 of 1.15 times, and for study 4 of 1.17 times the CM with respect to the NM. The greatest difference is given at $P_1 = 1000$ kN for study 3 of 1.20 times, and for study 4 of 1.10 times the NM with respect to the CM.

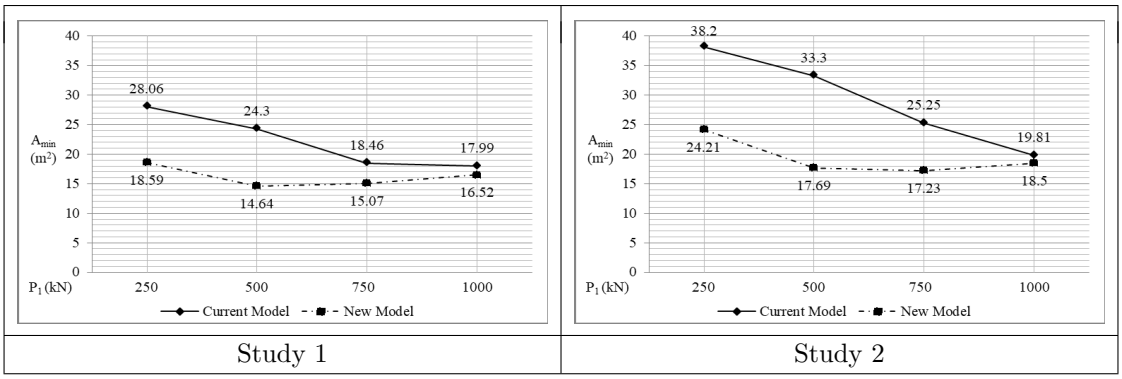

Study 1 | Study 2

FIGURE 7. Comparison of minimum areas for uniaxial bending of the two models with $M_{x1} = M_{x2} = 0$ kN-m

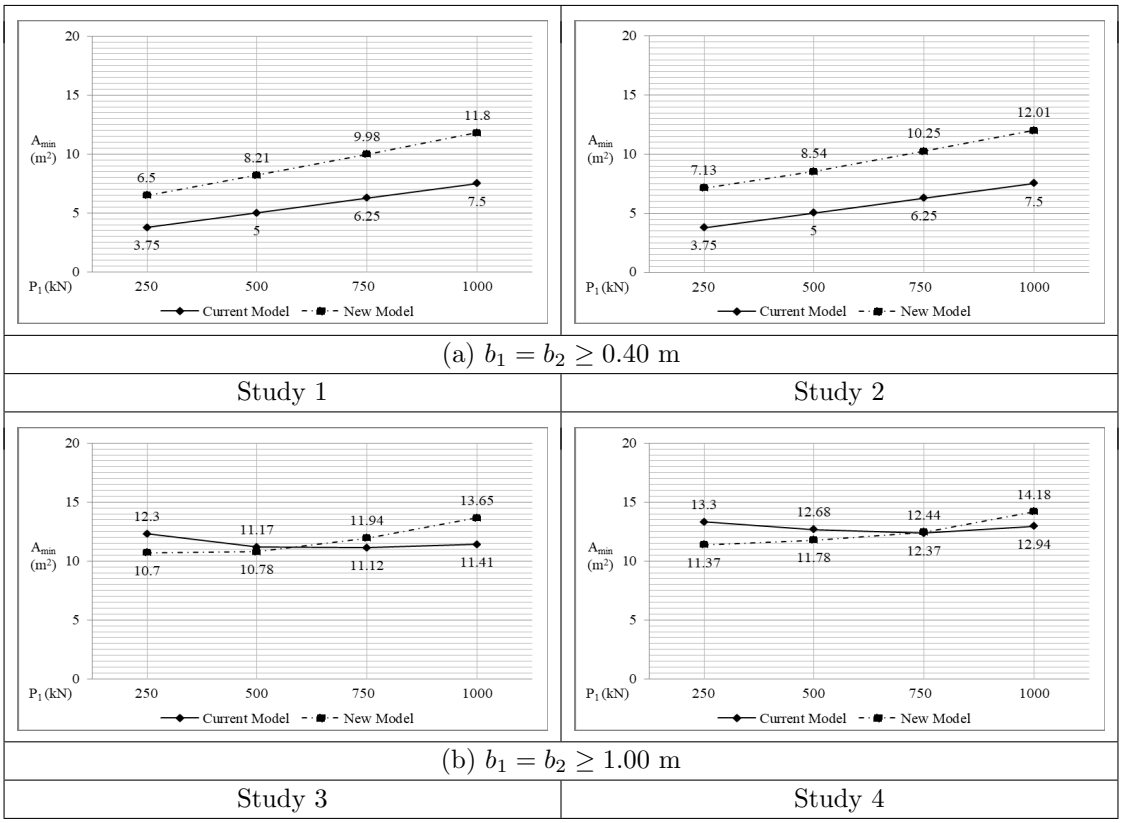

(a) $b_1 = b_2 \geq 0.40$ m

Study 1 | Study 2

(b) $b_1 = b_2 \geq 1.00$ m

Study 3 | Study 4

FIGURE 8. Comparison of minimum areas for uniaxial bending of the two models with $M_{y1} = M_{y2} = 0$ kN-m

5. **Conclusions.** Foundation of a structure is the essential part for transmitting the loads from the columns or walls to the underlying soil below the structure. The study of TCFs shown in this article produces exceptionally accurate results for all foundation engineering work. The main part of this work is to determine the minimum area of the TCFs.

This study assumes that the soil support layers are elastic and the footing is rigid, and the pressure diagram is presented as a linear variation.

Equations (19), (21), (23), (25), (27), (29), (31), (33), (35), (37), (39), (41), (46) and (48) can be verified using the geometric properties of a triangular-based pyramid to obtain the resultant force "R", the moment about the X axis "M_{xT}" and the moment about the Y axis "M_{yT}".

The main conclusions are the following.

1) Some authors propose equations to determine the sides of the footing and the minimum area, but they only consider case I (area is completely compressed).

2) The proposed model shows the precise and simplified equations and also presents the minimum area for each case.

3) The model can be used as a review of the allowable load capacity of the soil, taking account of the objective "$\sigma_{\max}$", and the same constraints for biaxial bending or uniaxial bending.

4) The proposed model for biaxial bending shows a significant saving in the minimum contact area on the ground of up to 65.30% less than the current model as can be seen in Figures 6(b) and 6(d).

5) The proposed model for uniaxial bending ($M_{x1} = M_{x2} = 0$ kN-m with unconstrained sides) shows a significant saving in the minimum contact area on the ground of up to 48.68% less than the current model as can be seen in Figure 7 in study 2.

6) When the pressure under the footing is uniform, it is governed by case I as can be seen in Figure 8(a).

7) When the resultant force increases, it tends to shift from the new model to the current model.

8) When the footing area is partially compressed, less earth extraction volume is generated, and therefore, the cost is reduced.

This study presents a robust and effective solution that is applied only to obtaining the sides and the minimum area of TCFs that rest on elastic soil, and the soil pressure on the footing is linear.

Suggestions for next investigations can be minimum design cost for TCFs considering that the area is partially compressed.

REFERENCES

[1] W. S. Abdullah, New elastoplastic method for calculating the contact pressure distribution, *Jordan Journal of Civil Engineering*, vol.2, no.1, pp.71-89, 2008.

[2] A. Luévanos-Rojas, A comparative study for dimensioning of footings with respect to the contact surface on soil, *International Journal of Innovative Computing, Information and Control*, vol.10, no.4, pp.1313-1326, 2014.

[3] G. A. Vyacheslavovich and B. L. Adolfovich, Influence of the form and size of the isolated foundations on the stress-strain state of the soil base, *Journal of Applied Engineering Science*, vol.14, no.1, pp.28-35, 2016.

[4] S. López-Chavarría, A. Luévanos-Rojas and M. Medina-Elizondo, A mathematical model for dimensioning of square isolated footings using optimization techniques: General case, *International Journal of Innovative Computing, Information and Control*, vol.13, no.1, pp.67-74, 2017.

[5] W. L. Filho, R. C. Carvalho, A. L. Christoforo and F. A. R. Lahr, Dimensioning of isolated footing submitted to the under biaxial bending considering the low concrete consumption, *International Journal of Materials Engineering*, vol.7, no.1, pp.1-11, 2017.

[6] S. Rawat, R. K. Mittal and G. Muthukumar, Isolated rectangular footings under biaxial bending: A critical appraisal and simplified analysis methodology, *Practice Periodical on Structural Design and Construction*, vol.25, no.3, 04020011, 2020.

[7] C. G. Konapure and B. Vivek, Analysis of combined rectangular footing by Winkler's model and finite element method, *International Journal of Engineering and Innovative Technology*, vol.3, no.5, pp.128-132, 2013.

[8] V. Bhogade, L. S. Arkal, R. V. Bandgar and F. A. Kalekhan, Comparative study on conventional and simplified elastic analysis of rectangular combined footing, *International Journal of Research in Engineering and Technology*, vol.3, no.4, pp.422-427, 2014.

[9] A. Luévanos-Rojas, A new mathematical model for dimensioning of the boundary trapezoidal combined footings, *International Journal of Innovative Computing, Information and Control*, vol.11, no.4, pp.1269-1279, 2015.

[10] A. Luévanos-Rojas, A mathematical model for the dimensioning of combined footings of rectangular shape, *Revista Técnica de la Facultad de Ingeniería Universidad del Zulia*, vol.39, no.1, pp.3-9, 2016.
[11] S. López-Chavarría, A. Luévanos-Rojas and M. Medina-Elizondo, Optimal dimensioning for the corner combined footings, *Advances in Computational Design*, vol.2, no.2, pp.169-183, 2017.
[12] A. Luévanos-Rojas, S. López-Chavarría and M. Medina-Elizondo, A new model for T-shaped combined footings Part I: Optimal dimensioning, *Geomechanics and Engineering*, vol.14, no.1, pp.51-60, 2018.
[13] R. C. Ravi-Kumar, M. Satish-Kumar, M. Kondala-Rao and N. Gopika, Numerical analysis of rectangular combined footings resting on soil for contact pressure, *International Journal of Civil Engineering and Technology*, vol.9, no.9, pp.1425-1431, 2018.
[14] G. Aguilera-Mancilla, A. Luévanos-Rojas, S. López-Chavarría and M. Medina-Elizondo, Modeling for the strap combined footings Part I: Optimal dimensioning, *Steel and Composite Structures*, vol.30, no.2, pp.97-108, 2019.
[15] A. I. Pasillas-Orona, A. Luévanos-Rojas, S. López-Chavarría, M. Medina-Elizondo and G. Aguilera-Mancilla, An optimized model for trapezoidal combined footings supported on the ground: Optimum surface, *Acta Universitaria*, vol.30, e2973, pp.1-18, 2020.
[16] M. A. Moreno-Hernandez, A. Luévanos-Rojas, S. López-Chavarría and M. Medina-Elizondo, Mathematical modeling for corner strap combined footings resting on the ground: Part 1, *Computación y Sistemas*, vol.26, no.3, pp.1259-1272, 2022.
[17] M. I. L. Ávila-García, A. Luévanos-Rojas, C. Martinez-Aguilar and L. L. Gaona-Tamez, Optimal area for rectangular foundation slabs in plan supported on soil, *International Journal of Innovative Computing, Information and Control*, vol.20, no.5, pp.1399-1413, 2024.
[18] R. Irles-Más and F. Irles-Más, Explicit stresses under rectangular detached footings with biaxial bending, *Informes de la Construcción*, vol.44, no.419, pp.77-90, 1992.
[19] H. M. Algin, Stresses from linearly distributed pressures over rectangular areas, *International Journal Numerical Analytical Methods in Geomechanics*, vol.24, no.8, pp.681-692, 2000.
[20] H. M. Algin, Practical formula for dimensioning a rectangular footing, *Engineering Structures*, vol.29, no.6, pp.1128-1134, 2007.
[21] G. Özmen, Determination of base stresses in rectangular footings under biaxial bending, *Teknik Dergi Digest*, vol.22, no.4, pp.1519-1535, 2011.
[22] I. Aydogdu, New iterative method to calculate base stress of footings under biaxial bending, *International Journal of Engineering & Applied Sciences (IJEAS)*, vol.8, no.4, pp.40-48, 2016.
[23] K. Girgin, Simplified formulations for the determination of rotational spring constants in rigid spread footings resting on tensionless soil, *Journal of Civil Engineering and Management*, vol.23, no.4, pp.464-474, 2017.
[24] V. B. Vela-Moreno, A. Luévanos-Rojas, S. López-Chavarría, M. Medina-Elizondo, R. Sandoval-Rivas and C. Martínez-Aguilar, Optimal area for rectangular isolated footings considering that contact surface works partially to compression, *Structural Engineering and Mechanics*, vol.84, no.4, pp.561-573, 2022.
[25] V. M. Moreno-Landeros, A. Luévanos-Rojas, G. Santiago-Hurtado, L. D. López-León and E. R. Diaz-Gurrola, Optimal area for a rectangular isolated footing with an eccentric column and partial ground compression, *Applied Sciences*, vol.14, no.15, pp.1-16, 2024.
[26] S. Soto-Garcia, A. Luévanos-Rojas, J. D. Barquero-Cabrero, S. López-Chavarría, M. Medina-Elizondo, O. M. Farias-Montemayor and C. Martínez-Aguilar, A new model for the contact surface with soil of circular isolated footings considering that the contact surface works partially under compression, *International Journal of Innovative Computing, Information and Control*, vol.18, no.4, pp.1103-1116, 2022.
[27] I. Luévanos-Soto, A. Luévanos-Rojas, V. M. Moreno-Landeros and G. Santiago-Hurtado, Minimum area for circular isolated footings with eccentric column taking into account that the surface in contact with the ground works partially in compression, *Coupled Systems Mechanics*, vol.13, no.3, pp.201-217, 2024.
[28] A. Luévanos-Rojas, B. L. Estrada-Mendoza and M. Juárez-Ramirez, Comparative study for minimum areas in contact with the ground of rectangular and circular isolated footings working partially under compression, *Boletín Ciencias de la Tierra*, vol.55, no.1, pp.85-98, 2024.
[29] P. Montes-Paramo, A. Luévanos-Rojas, S. López-Chavarría, M. Medina-Elizondo and R. Sandoval-Rivas, Optimal area for rectangular combined footings assuming that contact surface with the soil works partially to compression, *Ingeniería Investigación y Tecnología*, vol.24, no.2, pp.1-15, 2023.

[30] A. Luévanos-Rojas, B. L. Estrada-Mendoza and M. Juárez-Ramirez, Optimal area for T-shaped combined footing assuming that the contact area with the soil works partially in compression, *Boletín Ciencias de la Tierra*, vol.58, no.2, pp.51-71, 2025.
[31] A. Luévanos-Rojas, Optimal surface for corner combined footings assuming that the ground contact area works partially in compression considering that the maximum pressure is located at the corner of the footing: Part 1, *Advances in Concrete Construction*, vol.19, no.6, pp.349-362, 2025.
[32] A. Luévanos-Rojas, Optimal surface for corner combined footings assuming that the ground contact area works partially in compression considering that the maximum pressure is located at one end and on the outer and inner side of the footing: Part 2, *Advances in Concrete Construction*, vol.19, no.6, pp.363-380, 2025.
[33] I. Luévanos-Soto, A. Luévanos-Rojas and R. M. Luévanos-Soto, Optimal surface in plan for strip footings assuming that the contact surface with soil works partially under compression, *International Journal of Innovative Computing, Information and Control*, vol.21, no.4, pp.937-953, 2025.

Author Biography

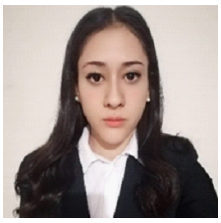

Rosa Margarita Luévanos-Soto received the Master's degree in Administration and Senior Management (2020) and the degree of Doctor in Administration and Senior Management (2024) from the Facultad de Contaduría y Administración of the Universidad Autónoma de Coahuila, México. She is professor and researcher of the Facultad de Contaduría y Administración, Torreón Campus of the Universidad Autónoma de Coahuila. Her research interests are mathematical models applied to Administration.

Arnulfo Luévanos-Rojas obtained his Bachelor's degree in Civil Engineering in 1981 from Facultad de Ingeniería, Ciencias y Arquitectura, Gómez Palacio Campus of the Universidad Juárez del Estado de Durango, México, his Master's degree in Science with Specialization in Structures in 1983 from Instituto Politécnico Nacional, Distrito Federal, México, his Master's degree in Science with Specialization in Planning and Construction of Works in 2000 from Facultad de Ingeniería, Ciencias y Arquitectura, Gómez Palacio Campus of the Universidad Juárez del Estado de Durango, México, his Master's degree in Administration in 2004 from Facultad de Contaduría y Administración, Torreón Campus of the Universidad Autónoma de Coahuila, México, and his Doctor degree in Engineering with Specialization in Planning Systems and Construction in 2009 from Facultad de Ingeniería, Ciencias y Arquitectura, Gómez Palacio Campus of the Universidad Juárez del Estado de Durango, México. He was professor and researcher of the Facultad de Ingeniería, Cienciasy Arquitectura, Gómez Palacio Campus of the Universidad Juárez del Estadode Durango, México from 2006 to 2015, and of the Facultad de Contaduría y Administración, Torreón Campus of the Universidad Autónoma de Coahuila, México, since 2015 to date. He has published more than 149 papers in journals indexed in the Web of Science. His research interests are mathematical models applied to engineering and administration. He is member of the National System of Researchers of Mexico (Level I from 2016-2022 and Level II from 2023-2027). He is an Honorary State Researcher for the State of Coahuila, México. He has received several distinctions: Distinguished Professor by ULSA (Universidad La Salle Laguna) 2002, 2007, 2010; Researcher of the year 2023 by UAC (Universidad Autónoma de Coahuila); Best scientific article of the year 2023 by UAC (Universidad Autónoma de Coahuila); He has been included in the "2023 World's Top 2% Scientists List" by Stanford University, Mathematical Engineering Excellence Award by "Math Scientist Awards" 2025, Best Researcher Award by "International Top Research Awards" 2025.

Inocencio Luévanos-Soto obtained his Bachelor's degree in Architect in 2009, his Master's degree in Science with Specialization in Planning and Construction of Works in 2012, and his Doctor degree in Engineering with Specialization in Planning Systems and Construction in 2024, all from Facultad de Ingeniería, Ciencias y Arquitectura, Gómez Palacio Campus of the Universidad Juárez del Estado de Durango, México. He is professor and researcher of the Facultad de Ingeniería, Ciencias y Arquitectura, Gómez Palacio Campus of the Universidad Juárez del Estado de Durango, México since 2010 to date. His research interests are mathematical models applied to engineering and architect.